Numerical Simulation Experiments on Water Seepage in Unsaturated, Heterogeneous Fractures

Tai-Sheng Liou [1,2], *Karsten Pruess* [1], *and Yoram Rubin* [2]

[1] Earth Science Division, Lawrence Berkeley Laboratory, University of California, Berkeley, California 94720
[2] Department of Civil and Environmental Engineering, University of California, Berkeley, California 94720

Abstract

In this paper, we discuss the study of unsaturated flow in fractures with a detailed resolution of heterogeneity. Fractures were simulated as two-dimensional porous media characterized by a heterogeneous and spatially correlated permeability field that was numerically generated by simulated annealing (SA). By introducing the concept of neighborhood into the Metropolis algorithm (Metropolis, 1953), we were able to capture the correlation structure near asperity contacts. Flow in such heterogeneous fractures was simulated by using the module EOS9 in TOUGH2. Simulation results showed that flow depends strongly on scales of heterogeneity and boundary conditions. Preferential flow paths, bypassing and ponding were observed in all realizations reported here. Increasing the percentage of asperity contacts resulted in more tortuous flow channels, but also significantly changed the breakthrough behavior and the seepage pattern.

Introduction

Fluid flow and solute transport in unsaturated, fractured rocks have generated increasing interest in recent years. The Department of Energy has been investigating the feasibility of building a repository for high-level nuclear waste at Yucca Mountain, an arid region near the Nevada-California border with the geological formation composed primarily of welded and non-welded tuffs having fractures with different scales of heterogeneity. The potential repository site at Yucca Mountain is approximately 375 m beneath the land surface and the water table is at a depth of approximately 600 m. Since fast preferential flow has been observed in a similar semi-arid environment at Rainier Mesa (Lawrence Berkeley National Laboratory, 1991), there is a concern that radionuclides released from canisters in the potential site at Yucca Mountain might be transported downward through fractures to the saturated zone. The focus of the present study is flow in heterogeneous fractures in order to understand water seepage and its implications in unsaturated fractured media such as are encountered at Yucca Mountain.

Naturally fractured rocks generally form a complex, three-dimensional network composed of interconnected and heterogeneous fractures. Predicting flow behavior in such media is generally difficult. One approach to understanding flow behavior in fracture networks is to simulate flow in a single fracture and extrapolate the results to the overall network (Nordqvist *et al.*, 1992). Thus, simulating flow in a single fracture is necessary for understanding flow and transport in naturally fractured rocks. The ultimate goals of this study are to interpret the unsaturated flow regime observed in the field and to provide guidelines for field experiments.

In this paper, we discuss the investigation of unsaturated flow in a single, vertical fracture plane. The heterogeneous and correlated permeability field in this fracture plane was generated with simulated annealing (SA) using a modified perturbation mechanism. The fracture plane was discretized into 10,000 square grid blocks with a grid block size of 0.2 m. This allows the applicability of the relative permeability and capillary pressure relationships based on the macroscale continuum concepts (Persoff and Pruess, 1995). Typical value of the matrix permeability for unfractured welded tuffs at Yucca Mountain is of order 10^{-18} m^2 or lower.

Therefore, impact of the matrix permeability on seepage pattern was neglected because of its much smaller magnitude than the reference permeability for fractures in welded tuffs (10^{-9} m^2), and the short timescale of interest (days). The isothermal flow of water was simulated by the general purpose simulator TOUGH2 (Pruess, 1991) with EOS9 module. EOS9 solves the Richards' equation, considering only single component aqueous phase flow and treating gas phase as a passive bystander. We focus on transient and steady state flows of water in unsaturated fractures under different boundary conditions. Also, we study the influence of the percentage of asperity contacts on the breakthrough behavior and seepage pattern. All flow simulations were performed on a personal computer with a Pentium-150 processor.

Heterogeneous Fractures

Simulated annealing (SA) was used to generate the heterogeneous permeability field in fractures. The algorithm of SA is based on an analogy between the physical process of annealing and the optimal ordering of a system with various components. Beginning with an initial state, SA perturbs the system by choosing one random pair at each perturbation and deciding whether exchanging the members of this pair is favored or not according to a particular perturbation mechanism, for example, Metropolis algorithm (Metropolis *et al.*, 1953). Annealing proceeds until the system reaches the state with the minimum global energy, or until the system energy cannot be further reduced. Here, the energy is a measure of the difference between the desired distribution and the realization of some spatial features. In this paper, we used the isotropic exponential semi-variogram model with nugget=0.0, sill=190.0 and integral scale=0.2 m to describe the spatial correlation structure. Details of SA can be found elsewhere, e.g., Deutsch and Journel (1992) and Deutsch and Cockerham (1994).

A vertical fracture plane 20 m wide by 20 m deep, and with a nominal thickness of 1cm, is discretized into 100×100 grid blocks, i.e., $\Delta x=\Delta z=0.2$ m. Permeability modifiers, ζ, are used to describe the permeability field according to $k = k_{ref} \times \zeta$, where k is the intrinsic permeability and k_{ref} is the reference permeability of $10^{-9}m^2$. The initial field for SA was synthesized by first generating the initial asperity contacts ($\zeta=0$), then filling-in non-conditioning grid blocks with univariate random numbers generated from a log-normal distribution with mean and standard deviation of the log-transformed ζ as 1.0 and 1.5, respectively. The initial asperity contacts were generated prior to SA and were used as the conditioning data. In order to have a gradual change of apertures near asperity contacts, the log-normal distribution was further shifted by a constant, Δ, i.e., $\zeta'=\max(\zeta-\Delta,0)$, such that additional unconditioning asperity contacts were produced. Because of the heterogeneity introduced by the permeability field, the capillary pressure is scaled by the factor $1/\sqrt{\zeta'}$ (Leverett, 1941).

Pruess and Antunez (1995) suggested that, for "small" fractures in hard rock, a realistic representation of heterogeneity should have the following characteristics: (1) the presence of asperity contacts; (2) a gradual change towards larger apertures away from the asperities; (3) a small-scale roughness of the fracture wall, and (4) a finite spatial correlation length among apertures. We found that the Metropolis algorithm was not adequate to capture the correlation structure near asperity contacts. Therefore, we modified the algorithm by introducing the concept of neighborhood such that the vicinity of conditioning asperity contacts can be emphasized. The neighborhood of a conditioning asperity contact is defined as the non-conditioning grid blocks that are at most 3 grid blocks away from the asperity contact. After investigating several possible combinations, we determined that the following algorithm is successful in annealing towards simply-connected asperities, i.e., if both of the data in a random pair are inside or outside of any neighborhoods, the Metropolis algorithm is still used; if only one of the data is in a neighborhood, this pair is unconditionally

accepted if the data outside the neighborhood has a smaller ζ than the one inside the neighborhood. We call this new algorithm the 'modified Metropolis algorithm'.

Figure 1 shows a typical realization annealed with the modified Metropolis algorithm for isotropic conditioning asperity contacts. The total percentage of asperity contacts was increased from 10% to 25%, i.e., Δ=0.64. This percentage was chosen heuristically based on fracture wall coating data from Yucca Mountain (Wang and Narasimham, 1985). Figure 2 shows the corresponding conditioning asperity contacts used in Figure 1. The spatial correlation structure and the clustering effects can be clearly seen in Figure 1. However, we found that visually distinctive permeability fields may give the same "perfect" match to the prescribed semi-variogram shown in Figure 3. This perfect match raised the issue of whether such a crude characterization of heterogeneity as is embodied in a semi-variogram is adequate for describing heterogeneous fractures. Despite its limitations, we used the semi-variogram as the correlation model in our simulations because of its simplicity and the lack of better correlation models in the literature.

Flow simulations

Variably saturated isothermal flow in heterogeneous fractures is described by the Richard' equation (Oldenburg and Pruess, 1993). This equation was solved using TOUGH2 with the module EOS9. EOS9 considers only single-component aqueous phase flow and treats gas phase as a bystander at constant pressure. The relative permeability and capillary pressure used in Richards' equation were expressed by van Genuchten's (1980) equations

$$k_{rl} = \sqrt{S^*}\left\{1-\left(1-\left[S^*\right]^{1/\lambda}\right)^{\lambda}\right\}^2, \quad P_{cap} = -P_0\left(\left[S^*\right]^{1/\lambda}-1\right)^{1-\lambda} \qquad (1),$$
$$S^* = (S_l - S_{lr})/(1-S_{lr})$$

where S^* is the effective saturation, S_l is the liquid (water) saturation, S_{lr} is the residual saturation, λ is a fitting parameter related to the pore-size distribution, and P_{cap} is the capillary pressure. Parameters used in Eq(1) were derived from a coarse sand material, i.e., λ=0.457, S_{lr}=0.15 for k_{rl} and S_{lr}=0.0 for P_{cap}, and P_0=195.9 Pa. The porosity of the medium was assumed to be 0.35 in all simulations, and the reference permeability was 10^{-9} m^2.

In the simulations reported here, water was initially at the residual saturation (S_{lr}), i.e., S_l=0.15. No-flow boundary conditions were assumed for lateral boundaries. Water was injected either locally at the center of the top boundary over a 1 m interval or uniformly over the entire top boundary. The injection rate was a constant 10^{-3} kg/s. For localized injection cases, no-flow boundary condition was assumed at the top boundary outside the injection region. To simulate the steady state flow in fractures far above the water table, a unit head gradient boundary condition was imposed at the bottom boundary. For simulating transient flow to the time of first breakthrough at the bottom boundary, no flow condition was assumed at the bottom boundary.

Figures 4 and 5 show transient flows in the fracture of Figure 1 for localized and uniform injection, respectively, at the time of breakthrough at the depth of -19.5 m. Flow evolves by gravity, capillarity and pressure force. Preferential flow paths are evident in both simulations, some of which pond upon some asperity contacts, merge with other flow paths, and keep evolving as they proceed downward. Flow ponding and bypassing caused by asperity contacts can be identified in both cases. For the localized injection case, the

breakthrough point may or may not be at the center of the bottom boundary. All the above phenomena are induced by the heterogeneity of the medium. Figures 4 and 5 show significantly different evolution of flows, indicating that flow behavior changes dramatically with different boundary conditions.

Figures 6 and 7 show unsaturated flows at steady state for localized and uniform injection, respectively. Here, an approximate "steady state" flow field is recognized when the ratio of the fluxes at the bottom to the top reaches 0.999. We noted that the saturation field continues to evolve even if the flux ratio exceeds 0.999 but at much slower time scales than in Figures 6 and 7. Figure 7 shows that some areas of the fracture will never be visited by water because of the heterogeneity of the medium.

Natural fractures may have more or less asperity contacts than was assumed in the above simulations. Experimental data (Raven and Gale, 1985) have demonstrated that increasing the contact areas in fractures results in more tortuous flow channels. This motivated us to study the effect of percentage of asperity contacts on the flow behavior. Figures 8, 9 and 10 show the steady state flow in the fracture plane of Figure 1 but with 15%, 35% and 40% asperity contacts, respectively. The effect of the percentage of asperity contacts on flow is evident. For better illustration of the effects of asperity contacts on flow behavior, the 35% and 40% asperity contacts are also superimposed on their corresponding flow fields in Figures 9 and 10, respectively. Figure 10 shows that only one finger reaches the bottom. In contrast, in Figures 7 and 8 water contacts almost the entire bottom boundary. Also, flow ponding increases with increasing percentage of asperity contacts.

Breakthrough curves are shown in Figure 11 for asperity contacts ranging between 15% and 40%. The curve becomes steeper as the percentage of asperity contacts increases. The breakthrough curve at 40% asperity contacts shows repeated cycles of fast and retarded breakthrough, suggesting that the breakthrough behavior is non-uniform and depends on the contact areas in fractures. The curves also show a general trend of faster breakthrough with increasing percentage of asperity contacts. Note that average vertical permeability decreases with increasing asperity contacts. Thus, we have the interesting result that seepage may proceed faster in fractures of lower average permeability. These results indicate that the breakthrough behavior as well as the seepage pattern are greatly influenced by the percentage of asperity contacts.

Conclusions

High resolution of the spatial discretization has enabled us to simulate the correlated heterogeneities in fractures on the scale of decimeters. Heterogeneous fractures generated by SA using a modified Metropolis algorithm were able to capture realistic correlation structure, especially near asperity contacts. Different scenarios of flow simulation showed complex flow phenomena like preferential flow paths, ponding, and bypassing, which are due to different scales of heterogeneity and boundary conditions. Results also implied that seepage pattern and breakthrough behavior depend strongly on the percentage of asperity contacts. Our numerical simulation experiments are consistent with field observations of preferential flow, and provide some insights into the flow and transport mechanisms within the fracture plane.

Acknowledgement

This work was funded by the Director, Office of Energy Research, Office of Health and Environmental Sciences, Biological and Environmental Research Program, of the U.S. Department of Energy under Contract No. DE-AC03-76SF00098. Thanks are due to Jil Geller and George J. Moridis for reviewing the manuscript and suggesting improvements.

References

Deutsch, C.V., and A. G. Journel, GSLIB, Geostatistical Software and User Guide, Oxford University Press, New York, 340p., 1992.

Deutsch, C. V., and P. W. Cockerham, Practical Considerations in the Application of Simulated annealing to Stochastic Simulation, *Mathematical Geology*, Vol. 26, No. 1, pp. 67-82, 1994.

Lawrence Berkeley National Laboratory, Geologic Repository Project, A Review of Rainier Mesa Tunnel and Borehole Data and Their Possible Implications to Yucca Mountain Site Study Plans, Lawrence Berkeley National Laboratory Report LBNL-32068, 99p., December 1991.

Leverett, M. C., Capillary Behavior in Porous Solids, *Trans. Soc. Pet. Eng. AIME*, Vol. 142, pp.152-169, 1941.

Metropolis, N., A. Rosenbluth, M. Rosenbluth, A. Teller, and M. Teller, Equations of State Calculations by Fast Computing Machines, *Journal of Chemical Physics*, Vol. 21, pp.1087-1092, 1953.

Nordqvist, A. W., Y. W. Tsang, C. F. Tsang, B. Dverstrop, and J. Anderson, A variable aperture fracture network model for flow and transport in fractured rocks, *Water Resou. Res.*, Vol. 28, No. 6, pp. 1703-1713, 1992.

Oldenburg, C. M., and K. Pruess, On Numerical Modeling of Capillary Barriers, *Water Resou. Res.,* Vol. 29, No. 4, pp. 1045-1056, 1993.

Persoff, P., and K. Pruess, On Numerical Modeling of Capillary Barriers, *Water Resou. Res.,* Vol. 31, No. 5, pp. 1175-1186, 1995.

Pruess, K., TOUGH2 - A General Purpose Numerical Simulator for Multiphase Fluid and Heat Flow, Report No. LBL-29400, Lawrence Berkeley Laboratory, Berkeley, CA, May 1991.

Pruess, K., and E. Antunez, Application of TOUGH2 to Infiltration of Liquids in Media with Strong Heterogeneity, Proceedings of the TOUGH Workshop '95, Lawrence Berkeley Laboratory Report LBL-37200, pp. 69-76, Berkeley, CA, March 1995.

Raven, K. G., and J. E. Gale, Water Flow in a Natural Rock Fracture as a Function of Stress and Sample size, *Int. J. Rock Mech. Sci. & Geomech. Abstr.*, Vol. 22, No. 4, pp. 251-261, pp. 1985.

van Genuchten, M. Th., A Closed-Form Equation for Predicting the Hydraulic Conductivity of Unsaturated Soils, *Soil Sci. Soc. Am. J.*, Vol. 44, p. 892-898, 1980.

Wang, J.S.Y., and T. N. Narasimhan, Hydrologic Mechanisms Governing Fluid Flow in A Partially Saturated, Fractured, Porous Medium, *Water Resou. Res.,*, Vol. 21(12), pp. 1861-1874, 1985.

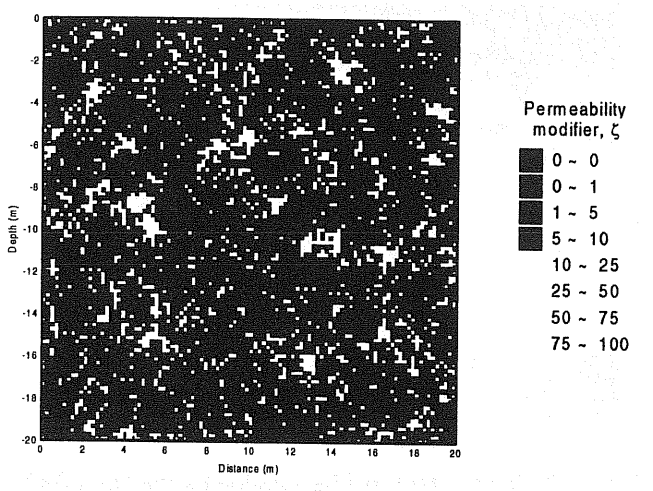

Figure 1. Permeability field generated with SA using the modified Metropolis algorithm and isotropic conditioning data. The percentage of asperity contacts is 25%.

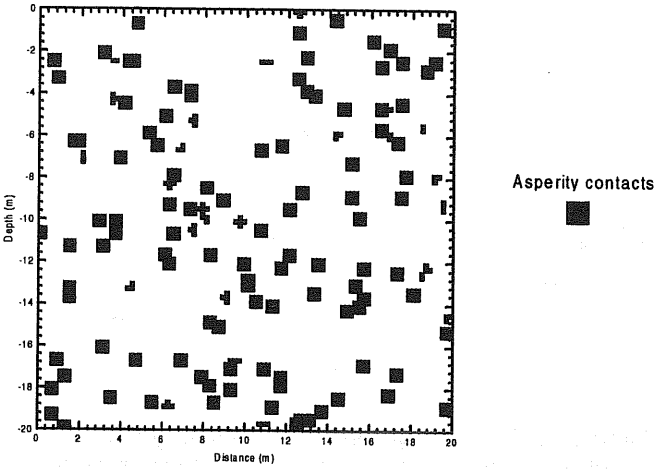

Figure 2. Asperity contacts used as the initial conditioning points for the permeability field in Figure 1. The percentage of conditioning asperity contacts is 10%.

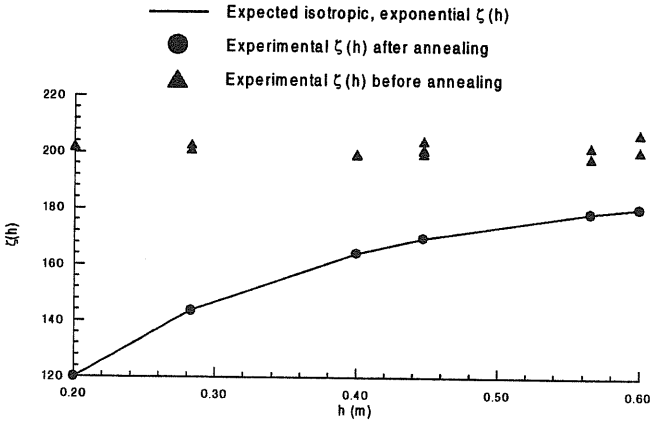

Figure 3. Expected and simulated spatial correlation relationships for the permeability field shown in Figure 1.

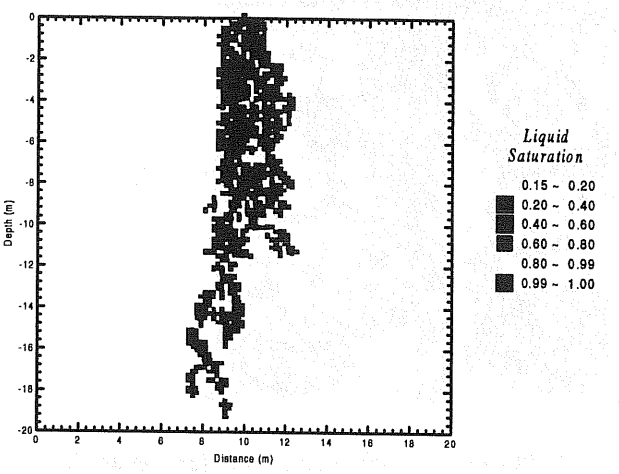

Figure 4. Liquid saturation for localized injection in fracture of Figure 1 at the time of first breakthrough at the depth of -19.5 m (Time=14.36 hrs).

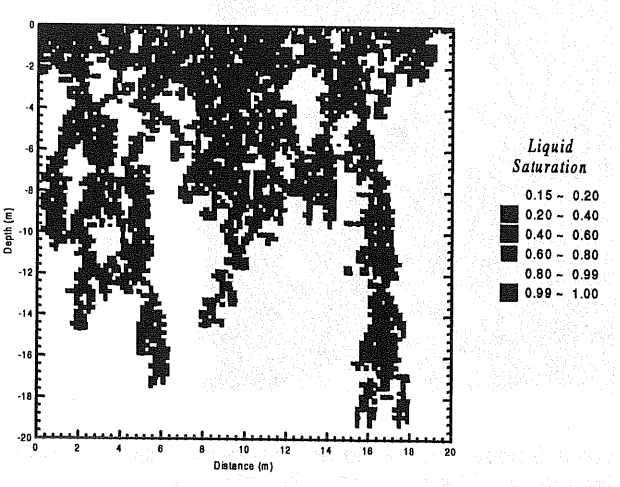

Figure 5. Liquid saturation for uniform injection in fracture of Figure 1 at the time of first breakthrough at the depth of -19.5 m (Time=40.85 hrs).

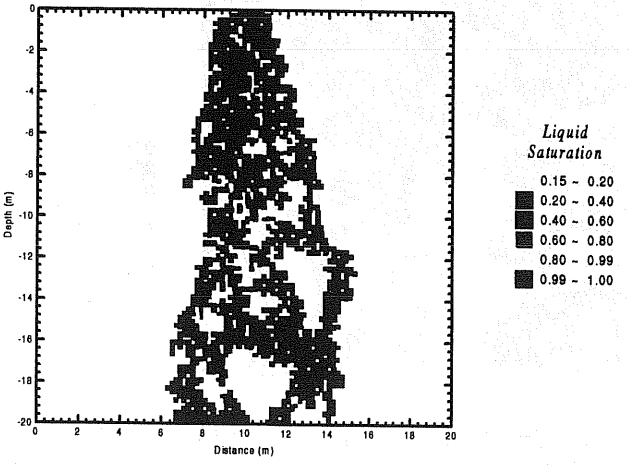

Figure 6. Steady state liquid saturation for localized injection in fracture of Figure 1. Simulation time=9.73 days.

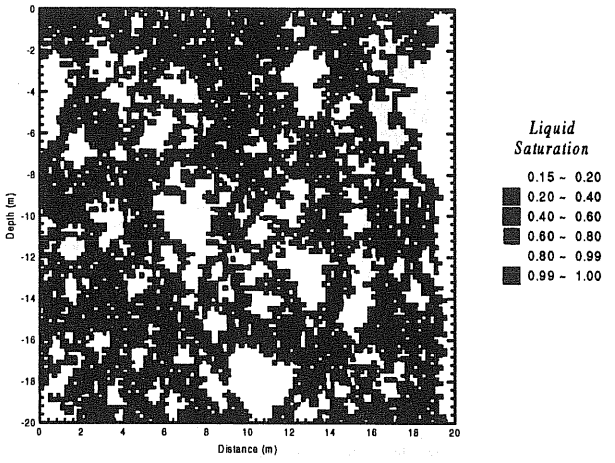

Figure 7. Steady state liquid saturation for uniform injection in fracture of Figure 1 with 25% asperity contacts. Simulation time = 55.56 days.

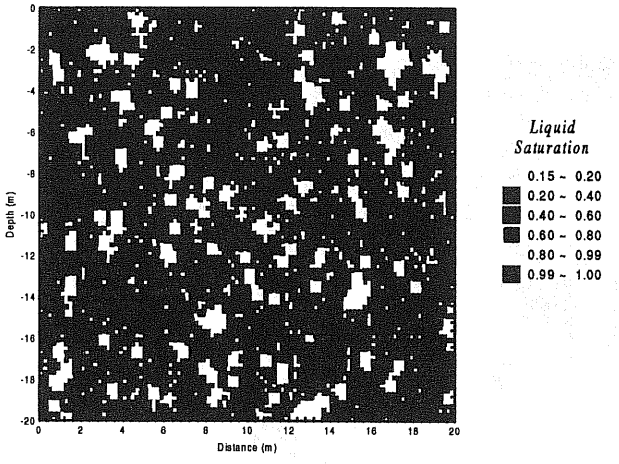

Figure 8 Steady state liquid saturation for uniform injection in fracture of Figure 1 but with 15% asperity contacts. Simulation time = 15.31 days.

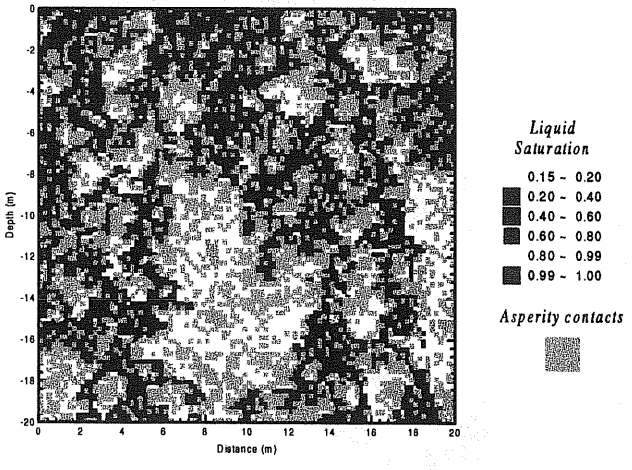

Figure 9. Steady state liquid saturation for uniform injection in fracture of Figure 1 but with 35% asperity contacts. Simulation time = 49.00 days.

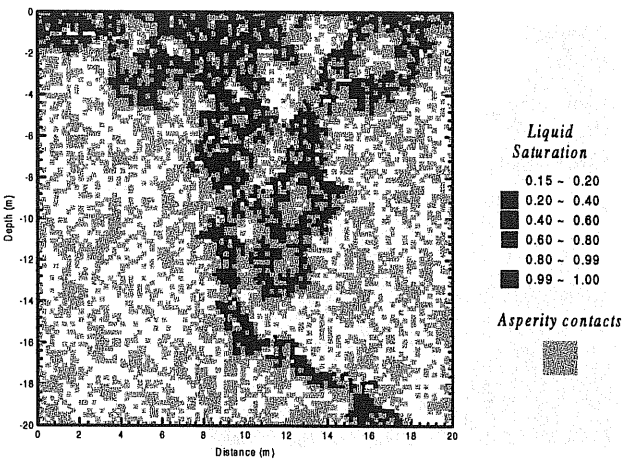

Figure 10. Steady state liquid saturation for uniform injection in fracture of Figure 1 but with 40% asperity contacts. Simulation time = 9,96 days.

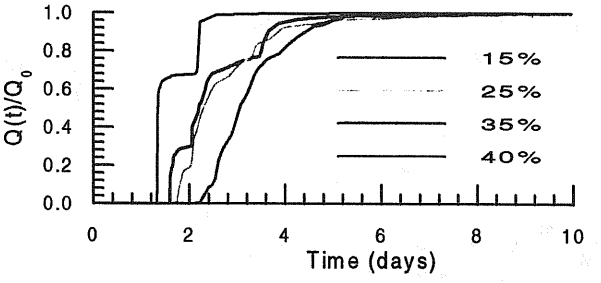

Figure 11. Breakthrough curves of the steady flow fields for the uniform injection cases with different total percentage of asperity contacts.